The influence of $BaSnO_3$ and $BaZrO_3$ nanoinclusions on the critical current and local structure of HTS coated conductors

A P Menushenkov[1], A.A. Ivanov[1], O V Chernysheva[1], I A Rudnev[1], M A Osipov[1], A R Kaul[2] V N Chepikov[2], O Mathon[3], V Monteseguro[4], F d'Acapito[5], A Puri[5]

E-mail: APMenushenkov@mephi.ru

[1] National Research Nuclear University MEPhI (Moscow Engineering Physics Institute), Moscow, 115409, Russia

[2] Lomonosov Moscow State University, Moscow, 119991, Russia

[3] ESRF, The European Synchrotron, CS40220, F-38043 Grenoble Cedex 9, France

[4] DCITIMAC, Universidad de Cantabria, Avenida de los Castros 48, 39005 Santander, Spain

[5] Consiglio Nazionale delle Ricerche – Istituto Officina dei Materiali – Operative Group in Grenoble at European Synchrotron Radiation Facility, Linea Italiana per la Spettroscopia d'Assorbimento Collaborating Research Groups, 38000 Grenoble, France

Abstract. We studied the effect of artificial pinning centers in the form of nanoinclusions of stannate $BaSnO_3$ (BSO) and zirconate $BaZrO_3$ (BZO) barium on the critical current of high-temperature superconducting tapes of the second generation (2G) based on $YBa_2Cu_3O_{7-\delta}$ films (YBCO). It has been found that the introduction of $BaZrO_3$ nanoinclusions increases the critical current at 77 K for the magnetic field direction parallel and normal to the tape surface, while the introduction of $BaSnO_3$ nanoinclusions decreases the critical current in both cases. To elucidate the origin of a different impact of nanoinclusions we examined the local structure of the YBCO-matrix using x-ray absorption spectroscopy (EXAFS and XANES). The spectra were collected at K-edges of Cu, Sn, and Zr at the European Synchrotron (ESRF). It was revealed that the introduction of $BaZrO_3$ nanoinclusions increases the stiffness of copper - oxygen bonds in superconducting CuO_2 plane and minimizes their static disorder in the YBCO matrix, while the introduction of $BaSnO_3$ nanoinclusions leads to a significant increase in static disorder with a relatively weak effect on the stiffness of Cu – O bonds. These changes in the local structure become decisive for changing the macroscopic properties of HTSC - tapes.

Submitted to: *Supercond. Sci. Technol.*

Keywords: critical current, EXAFS, XANES, YBCO-matrix, nanoinclusions, pinning, MOCVD

1. Introduction

The $REBa_2Cu_3O_{7-\delta}$ compounds (REBCO, where RE is a rare earth element) belong to the family of cuprate high-temperature superconductors (HTSC) and form a group of ceramic superconducting materials most important for practical applications. These compounds are used to fabricate composite superconducting materials - HTSC tapes of the second generation and wires based on them [1, 2, 3]. The critical current J_c, which is the most important practical characteristic of a superconductor, as well as the dependence of the critical current on the applied magnetic field $J_c(H)$, can be improved by adding the artificial pinning centers using various methods, for example, introducing the multilayered structure [4], irradiating by heavy ions [5] or fabricating a pattern of microholes [6], magnetic dot arrays [7], etc. One of such methods is the introduction of non-superconducting nanoinclusions into the superconducting matrix, which under certain conditions can play the role of additional artificial pinning centers and lead to an increase in the critical current [8, 9, 10]. Nanoparticles must meet two main criteria: first, they must not significantly decrease the critical temperature T_c, and second, their characteristic size must be of the order of the coherence length.

Most often, oxides of tetravalent metals M (M = Zr, Hf, Ce, Ti, and Sn) are used as nanoadditives to HTSCs. They form nanoscale inclusions of $BaMO_3$ perovskite phases in the REBCO matrix [11, 12]. The most common uses are barium stannate and zirconate. In particular, in the works [13, 14] it was shown that $BaZrO_3$ nanoparticles have good prospects for use as chemically inert (with respect to the HTSC matrix) pinning centers.

Studies on the introduction of nanoadditives as pinning centers were carried out for a wide range of methods for the synthesis of HTSC films: pulsed laser deposition (PLD - Pulse Laser Deposition) [15, 16], deposition from liquid organometallic precursors (MOD - Metalorganic Deposition) [17, 18], gaseous deposition using organometallic compounds (MOCVD - Metalorganic Chemical Vapor Deposition) [11, 12, 19, 20, 21, 22]. Along with monoadditives, the combinations of point and columnar defects were also considered [23]. A well-known example of such a combination is $BaZrO_3$(BZO) and Y_2O_3 [24, 25], and $BaSnO_3$(BSO) [26].

It was shown that $BaZrO_3$ inclusions in thin HTSC films are assembled into self-organized structures in the form of columnar defects - nanocolumns elongated along the normal to the film surface, which work especially well as pinning centers in a perpendicular magnetic field [16, 19, 20]. In the work [20], the effect of the concentration of $BaZrO_3$ nanoinclusions on the magnetic and electrical transport properties of the second generation HTSC tapes produced by SuperPower Inc. using the MOCVD technique was studied in detail. It was shown that the optimal content of $BaZrO_3$ is about 5 % mol.

Artificial pinning centers based on $BaZrO_3$ and $BaSnO_3$ have the greatest effect on the properties of HTSC at low temperatures and high magnetic fields [26, 27, 28]. However, the enhancement of the pinning effect in HTSCs doped with $BaZrO_3$ is also

noticeable at higher temperatures [29].

To gain insight into the nature of the influence of pinning nanoinclusions on the critical characteristics of HTSC, it is necessary to study their impact on the structure of a superconductor. There are several publications on the microstructure of REBCO composites with $BaZrO_3$ [21, 26, 27, 30, 31, 32] and $BaSnO_3$ [22, 26, 27, 33]. Transmission electron microscopy [30] and x-ray diffraction [21, 31, 32] are actively used for this purpose. However, there are few studies of the influence of nanoinclusions on the structure of a superconductor at the local level, and this effect needs further investigation so far. Thus, the study of HTSC tapes by x-ray absorption spectroscopy (EXAFS and XANES) gave additional evidence for the existence of zirconium nanoinclusions in the form of $BaZrO_3$ [19]. Prayoonphokkharat et al [22] found the secondary phase $BaSnO_3$ in tin-doped YBCO and proved using XANES spectroscopy that tin does not substitute for copper. Oh et al [33] reported the EXAFS study of $GdBa_2Cu_3O_{7-\delta}$ films with $BaSnO_3$ nanoinclusions fabricated using PLD. They concluded that the films have local oxygen deficiency at the apical position, depending on the film thickness and acting as additional pinning centres, which are most efficient for 0.8 μm-thick films.

However, at the moment there is no consistent comparative study of the impact of nanoinclusions $BaZrO_3$ and $BaSnO_3$ on the critical current and the local structure of identical HTSC-matrices, which would help to clarify the nature of their differences in the influence on the critical parameters of a superconductor.

In the previous study [34] we investigated the impact of nanoinclusions of $BaZrO_3$ on the local structure of YBCO matrix. We found the optimal content of nanoinclusions (5 mol %) and revealed a correlation between the local structure of the superconducting YBCO matrix and the critical current in HTSC tapes with $BaZrO_3$ additives. Namely, an increase in the stiffness of bond Cu – O, accompanied by a decrease in their local disorder, correlates well with an increase in the critical current.

Complementing the previous work and proceeding further, we set a goal, firstly, to compare the influence of artificial pinning centers on the critical current of HTSC tapes for identical YBCO matrices with nanoadditions of $BaSnO_3$ and $BaZrO_3$, fabricated under identical conditions using MOCVD. Secondly, to use XAFS spectroscopy to elucidate the origin of the different impact of two types of nanoinclusions on the critical current on a local scale.

2. Experimental methods

All samples were superconducting $YBa_2Cu_3O_{7-\delta}$ 2G tapes deposited on buffer layers with the following sequence (from the top to the substrate): $LaMnO_3/MgO/Y_2O_3/Al_2O_3$. The buffer layers were grown on the electropolished Hastelloy C276 tape. All buffer layers except MgO were deposited by magnetron sputtering. Amorphous Al_2O_3 and Y_2O_3 were used to obtain the low roughness required for MgO deposition using the IBAD technique. The biaxial texture formed in the MgO layer was inherited by the epitaxial $LaMnO_3$ layer.

Superconducting YBCO layers with a content of 5 mol.% $BaZrO_3$ and $BaSnO_3$ were obtained by metalorganic chemical vapour deposition (MOCVD) using $Y(thd)_3$, $Ba(thd)_2$* tetraglyme, $Cu(thd)_2$, $Zr(thd)_4$ and $Sn(thd)_4$ as precursors. A detailed description of the deposition process of YBCO films with the introduction of nanoinclusions, together with the results of the structure analysis by x-ray diffraction (XRD) and scanning electron microscopy (SEM), is presented in [34] taking as an example the introduction of $BaZrO_3$ nanoinclusions.

To measure the critical current, which requires soldering metal contacts, the samples were coated with copper by electroplating. To study the local structure by x-ray absorption spectroscopy (XAFS), small fragments of each tape were taken, the upper protective silver layer was dissolved in a mixture of H_2O_2 and NH_4OH.

The x-ray absorption spectra were collected above the K absorption edges of Sn (29200.1 eV), Zr (17998 eV), and Cu (8978.9 eV) at the BM-23 [35] and BM-08 (LISA) [36] beamlines of the European Synchrotron Radiation Facility (Grenoble, France) in the fluorescence mode using a highly sensitive 13-element Germanium Discrete Array Detector CANBERRA. The x-ray beam was perpendicular to the surface of the HTSC tape during measurements, which corresponded to the polarization $\mathbf{E}\|ab$ for the taken spectra. Double-crystal monochromators Si(311) and Si(111) were used for measuring at K-Sn, K-Zr, and K-Cu, respectively, with a slit of 0.3 mm, providing an energy resolution of $\sim$0.5 eV for XANES and $\sim$2 eV for EXAFS. The spectra were analyzed after correction for the self-absorption of fluorescence emission in accordance with [37]. Temperature measurements in the range of 20 – 300 K were carried out using a liquid helium continuous flow cryostat with temperature stability of $\pm$0.1 K at 20 K and $\pm$1 K at 300 K. For all the studied absorption edges, the length of the spectra in the k-space was 16 $Å^{-1}$. In order to collect statistics at each temperature, 4 spectra were measured with subsequent integration. The processing of the spectra of extended x-ray absorption fine structure (EXAFS) was carried out using the software packages VIPER[38] and IFEFFIT[39].

3. Results

3.1. The impact of nanoinclusions of $BaSnO_3$ and $BaZrO_3$ on the critical current density in YBCO at 77 K.

The critical temperature T_c and the critical current density J_c were measured by a standard four-probe method. The samples were 12 mm-wide and 30 mm-long. The value of the critical temperature T_c was determined from resistivity measurements and for the sample without additives was 89.8 K. The critical current was measured at T=77 K in the range of magnetic field of 0 – 8 T for two directions of the magnetic field: parallel and perpendicular to the plane of the tape. The value of the critical current was determined from the I-V curves according to the criterion of 1 μV/cm. Fig. 1 shows on a double logarithmic scale the obtained dependences of the critical current density

on both directions of the applied magnetic field J_c(H) for the pure YBCO tape, and for tapes with BSO and BZO inclusions.

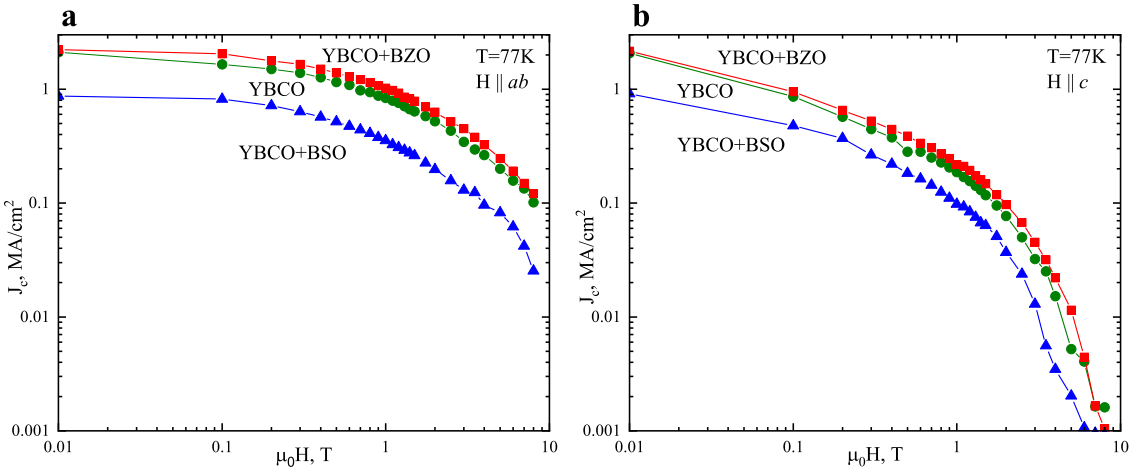

Figure 1. Dependence of the critical current density of the initial superconducting YBCO tape and tapes with nanoinclusions of barium stannate (BSO) and zirconate (BZO) on the induction of a magnetic field applied a) parallel (H ∥ *ab*) and b) perpendicular (H ∥ *c*) to the tape surface at T=77 K. The concentration of nanoinclusions of both types was 5 mol.%.

Based on the Dew-Hughes scaling law [40], we calculated field dependences of the pinning force F_p (F_p=$J_c \times \mu_0$H) in magnetic field perpendicular to the tape surface for three samples (pure YBCO and YBCO with BZO and BSO nanoinclusions).The pinning force was further normalized by F_p(max) and magnetic field was normalized by irreversibility field H_{irr}(taken as 8 T) h=H/H_{irr}. The resulting normalized dependences F_p/F_p(max) *vs* h have pronounced dome-like shape (Fig. 2). The position of the maximum is almost the same for all samples under study which means that the pinning mechanism in tapes with both types of nanoinclusions is the same as in pure YBCO tapes according to [40]. A similar analysis for direction H∥*ab* is complicated by high values of irreversibility field (when the critical current drops to zero), which were not achieved in our measurements.

3.2. XAFS spectroscopy results

The XAFS spectroscopy study, presented in [34], revealed that zirconium, introduced into the YBCO matrix, forms barium zirconate $BaZrO_3$. Literature data (see, for example, [22, 26, 27]) indicate a similar type of nanoinclusions of tin compounds at concentrations exceeding 0.2 mol%. In order to specify the structure of tin nanoinclusions in the YBCO superconducting matrix, XANES and EXAFS spectra collected at the *K*-Sn absorption edge were analyzed. The spectra at the *K*-edge of Sn for $BaSnO_3$ polycrystalline powders were also taken in the transmission mode as a reference. The *K*-Sn XANES spectra for the pure $BaSnO_3$ and the YBCO matrix with nanoinclusions are given in Fig. 3a), where one can clearly see that they are quite

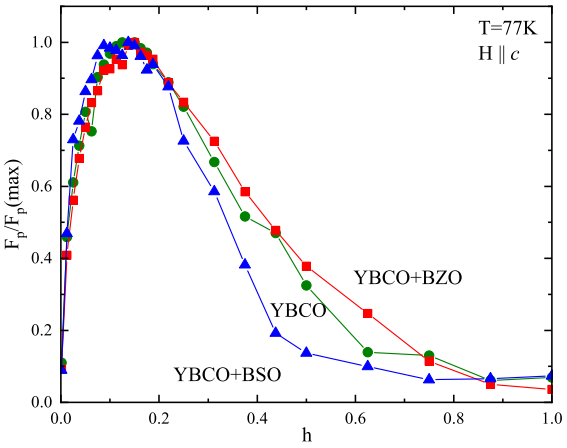

Figure 2. The normalized pinning force $F_p/F_p(\max)$ *vs* normalized magnetic field $h=H/H_{irr}$ measured at T=77 K. The magnetic field is perpendicular to the surface of the tape (H ∥ *c*). The concentration of nanoinclusions of both types was 5 mol.%.

similar. At the same time, they strongly differ from *K*-Sn XANES spectra of SnO_2 or other possible Sn-based compounds that could be formed during the film growth with nanoinclusions. The shape of the white line repeats that for pure $BaSnO_3$, except for a slight decrease in the intensity of the first peak, which may be associated with an increase in the local disorder of the local environment. Thus, the XANES study confirms that Sn is introduced into the YBCO matrix in the form of barium stannate $BaSnO_3$.

A similar conclusion concerning the presence of Zr in the form of $BaZrO_3$ was drawn from comparing the XANES spectra at the *K*-Zr absorption edge [34]. However, the intensity of the white line does not decrease in this case.

Additional evidence of the presence of Sn in the YBCO matrix in the form of $BaSnO_3$ nanoinclusions comes from the analysis of EXAFS spectra. Figure 3b) shows the Fourier transform modules (FT) of the k^2-weighted EXAFS functions $\chi(k)k^2$ measured above the Sn *K*-edge for pure $BaSnO_3$ powder and for the YBCO tape with $BaSnO_3$ nanoinclusions. Each FT peak corresponds to the nearest coordination shells of the Sn as follows: Sn – O, Sn – Ba, Sn – Sn. Here and further one should bear in mind that the distances in the Fourier transform differ from the real values due to the backscattering phase shift of the photoelectron wave. The correct values of the distances, given in Table. 1, were extracted after fitting the model EXAFS function to the experimental one. It is obvious that the number and position of the FT peaks for the case of $BaSnO_3$ nanoinclusions coincide with the FT peaks for the pure $BaSnO_3$. Since the shape of the Fourier transform module of the EXAFS function resembles a pair radial distribution function of atoms, from the changes in its shape one can qualitatively judge the differences in the local structure in the samples under study. For $BaSnO_3$ nanoinclusions, as well as for $BaZrO_3$ nanoinclusions [34], there is a decrease in the amplitude of the first peak of the FT module and a shift towards smaller values of R compared to the reference samples. The observed difference in peak amplitude indicates

the presence of a local structural disorder inside the nanoinclusions.

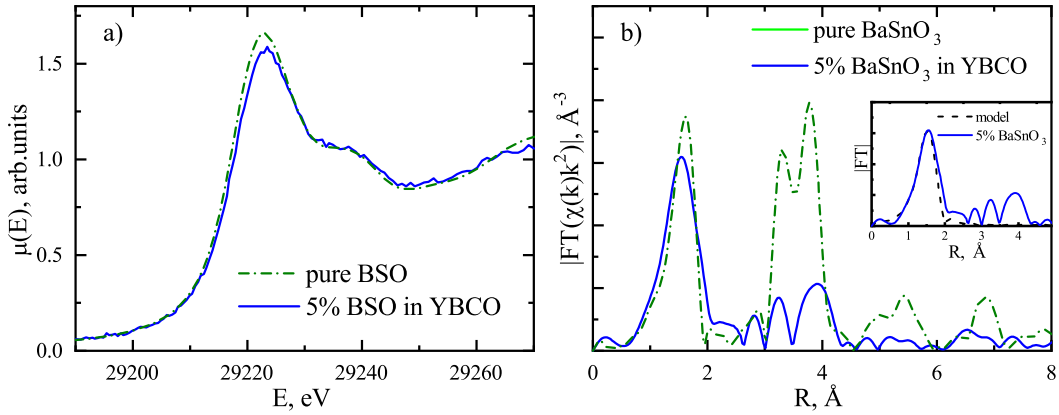

Figure 3. *K*-Sn XANES spectra (a) and Fourier transform modules *K*-Sn EXAFS spectra (b) for $BaSnO_3$ in a YBCO matrix and $BaSnO_3$ powder at 300 K. The inset in (b) shows the fitting of the first coordination shell Sn – O.

A shift means a decrease in the radius of the first coordination shell. It is also worth noting that the decrease in the height of the following peaks corresponding to the next coordination shells is more pronounced, which indicates a stronger disorder in the coordination shells Sn – Ba, Sn – Sn compared to the pristine sample. This may originate from the compression of the lattice of the nanoinclusions due to the semi-coherent interface with the HTSC matrix, as well as the reduction of particle size to nanoscale when incorporated into the YBCO matrix. The fitting of the experimental spectra made it possible to extract the radii of the first coordination shell and the Debye–Waller factors (D-W), which describe the standard deviation of the interatomic distance from its average value and characterizes the local disorder. In $BaSnO_3$ nanoinclusions, the coordination radius of the first shell decreases by 0.02 Å compared to $BaSnO_3$ powder, and the D-W factor increases by 0.002 Å^2 (Table. 1), which confirms the qualitative analysis. A similar situation is observed at the Zr *K*-edge.

Table 1. The parameters of the first coordination shell *M*-O for Sn and Zr in $BaSnO_3$ and $BaZrO_3$ nanoinclusions, respectively at T=77 K.

sample	R, Å	σ^2, Å^2
$BaSnO_3$	2.061(8)	0.0028(5)
5% $BaSnO_3$ in YBCO	2.041(8)	0.0060(6)
$BaZrO_3$	2.088(9)	0.0041(6)
5% $BaZrO_3$ in YBCO	2.080(9)	0.0070(6)

The numbers in parentheses are the estimated standard deviations (esd) obtained from the least-squares fits, R - a distance between M and O, σ^2 - the Debye -Waller factor.

Fig. 4 shows k^2-weighted *K*-Cu EXAFS functions $\chi(k)k^2$ (a) and the Fourier

transform modules of EXAFS spectra (b) measured at a temperature of 77 K for the pure YBCO matrix and the matrix with nanoinclusions of $BaSnO_3$ and $BaZrO_3$. One can see from Fig. 4b) that for $BaSnO_3$ the amplitude of all peaks of the Fourier transform module is smaller than for the pure YBCO matrix and the matrix with the addition of $BaZrO_3$. The peak positions for all three samples are almost the same.

When analyzing the Cu K-edge absorption spectra, we focused on the behavior of Cu – O bonds, since they are most important for the superconducting properties of HTSC cuprates [41, 42, 43, 44, 45]. Therefore, using the Hanning window, we selected the region corresponding to the first Cu – O shell in the Fourier transform (FT) of EXAFS function $\chi(k)k^2$. Next, we performed the inverse Fourier transform and thus restored the experimental EXAFS spectrum from the nearest oxygen shells, the so-called filtered EXAFS function. The spectra were fitted in k-space following the standard EXAFS formula obtained in the approximation of harmonic vibrations of atoms in the framework of the Einstein model, which according to [46] has some advantages over the Debye model when analyzing the first coordination shell of identical atoms. The amplitudes and phase shifts of backscattering were calculated from the first principles based on the theory of a self-consistent field embedded in the FEFF9[47] program code, while the structure was calculated on the basis of x-ray diffraction data. Since copper atoms occupy two different positions in the crystal structure of $YBa_2Cu_3O_{7-\delta}$, the first coordination shell Cu – O in the Fourier image (FT) includes several short ($\sim$1.9Å) distances: Cu(2) – O(2,3) inside the ab plane and Cu(1) – O(1) in the chain structure along the b axis (in the notation [48] for the superconducting orthorhombic phase YBCO). The longer apical bond Cu(2) – O(4) ($\sim$2.3 Å) and the bond Cu(1) – O(4) along the c axis do not contribute to the measured EXAFS function due to the linear polarization of synchrotron radiation along the tape plane ($\mathbf{E} \| ab$). Since the lengths of bonds Cu(2) – O(2,3) and Cu(1) – O(1,4) are very similar, we considered them one bond Cu – O of the average length in a single-shell model.

By fitting the experimental spectra, we have obtained the temperature dependences of the radii of the nearest coordination shells Cu – O and their Debye-Waller factors in the YBCO matrix (see Table. 2, Fig. 5).

The analysis revealed that within the fitting error, the bond lengths almost do not change with temperature, which may indicate a small coefficient of thermal expansion of the nearest environment of Cu. Shown in Fig. 5, the temperature dependences of the Debye-Waller factor of bond Cu – O for the initial YBCO matrix and the matrix with nanoinclusions $BaSnO_3$ and $BaZrO_3$ include static and dynamic contributions, which can be separated based on the following formula:

$$\sigma^2(T) = \sigma^2_{stat} + \sigma^2_d(T), \tag{1}$$

The static contribution does not change with temperature, and the dynamic contribution associated with thermal vibrations of atoms is described in the framework of Einstein's

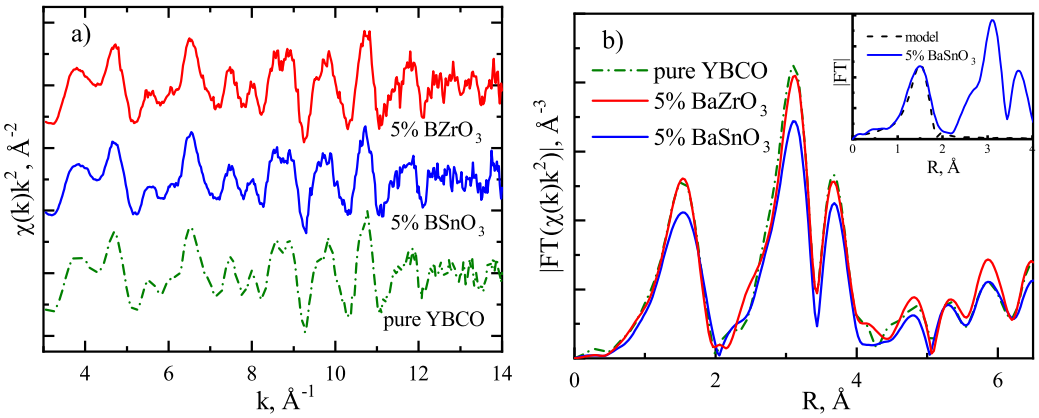

Figure 4. K-Cu EXAFS functions $\chi(k)k^2$ (a) and the Fourier transform modules of EXAFS spectra (b) for the initial YBCO matrix and the matrix with an optimal concentration of 5 mol% of $BaSnO_3$ and $BaZrO_3$ nanoinclusions measured at 77 K. The inset in (b) shows the fitting of the first coordination shell Cu – O for the matrix with $BaSnO_3$ nanoinclusions.

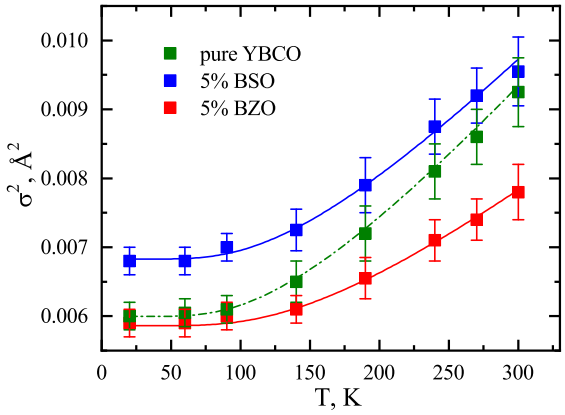

Figure 5. Temperature dependences of Debye-Waller factors for Cu – O coupling from the analysis of EXAFS spectra for the initial YBCO matrix and a matrix with an optimal concentration of 5 mol% of $BaSnO_3$ and $BaZrO_3$ nanoinclusions

harmonic model [46] as follows:

$$\sigma^2(T) = \sigma^2_{stat} + \frac{\hbar^2}{2k_B\mu}\frac{1}{T_E}\coth\left[\frac{T_E}{2T}\right], \tag{2}$$

Here $\hbar$ is Planck's constant, k_B is Boltzmann's constant, $T_E = \sqrt{k_{bond}/\mu}$ is the Einstein temperature expressed in terms of the bond stiffness k_{bond} and the reduced mass $\mu = mM/(m+M)$ of an ion pair with masses m and M. The static Debye-Waller factor σ^2_{stat} was determined by extrapolating the experimental dependence to T = 0 K minus the value $\sigma^2_d(0)$ corresponding to the amplitude of zero-point vibrations for a specific Einstein temperature [49].

The results of fitting (Table 2, Fig. 5) demonstrate that the nanoinclusions $BaSnO_3$ and $BaZrO_3$ affect the crystal lattice of the matrix at the local level. The Einstein temperature of the Cu – O bond in matrices with nanoinclusions turns out to be higher

than in the pristine one. This means that nanoinclusions of both types increase the stiffness of the bond, which should have a positive impact on the critical superconducting current.

Table 2. The parameters of the first coordination shell Cu – O for the initial YBCO matrix and matrices with an optimal concentration (5 mol%) of $BaSnO_3$ and $BaZrO_3$ nanoinclusions at T=77 K.

sample	R, Å	σ^2_{stat}, Å^2	$\sigma^2_{77\ K}$, Å^2	T_E, K
YBCO	1.89(1)	0.0060(1)	0.0061(1)	409(10)
5% $BaSnO_3$ in YBCO	1.90(1)	0.0068(1)	0.0069(1)	430(10)
5% $BaZrO_3$ in YBCO	1.88(1)	0.0059(1)	0.0059(1)	488(10)

The numbers in parentheses are the estimated standard deviations (esd) obtained from the least-squares fits, R - a distance between Cu and O, σ^2_{stat} - the static Debye -Waller factor.

However, in the case of $BaSnO_3$, the local disorder in Cu – O shells increases significantly. The D-W factor occurs to be greater in the entire temperature range, and the static D-W factor increases by $8{\cdot}10^{-4}$ Å^2 compared to the pure matrix and by $9{\cdot}10^{-4}$ Å^2 compared to the YBCO matrix with $BaZrO_3$ nanoinclusions. As a result, at 77 K, the critical current of the sample with $BaSnO_3$ turns out to be even less than the critical current of the pure YBCO matrix at both directions of the magnetic field (Fig. 1). Thus, it becomes clear that the influence of nanoinclusions on the static disorder of the Cu – O bond of the YBCO matrix plays a decisive role in improving the critical characteristics of the HTSC tape. A decrease in local disorder is an additional cause of an increase in the critical current in YBCO tape with $BaZrO_3$ nanoinclusions, whereas an increase in local disorder and the Cu – O bond in the YBCO matrix with $BaSnO_3$ nanoinclusions levels some increase in the stiffness of Cu – O bonds, which eventually leads to a decrease in J_c(77 K).

4. Discussion

The value of the critical current itself is a rather conditional parameter of the samples under study. In the general case, it is incorrect to compare by the magnitude of the critical current only the quality of samples of commercial HTSC-tapes based on a wide range of matrices such as YBCO [3, 11, 12, 13, 14, 15, 17, 34, 19], GdBCO [16, 26, 27, 33] and fabricated by a great variety of techniques, for example, PLD [12, 15, 26, 27] , MOCVD [11, 34, 19], MOD process [18], as well as thin films deposited on $SrTiO_3$ substrates of limited size using coprecipitation method [21], by solid-state synthesis [22] or by PLD [33]. The critical current primarily depends on the initial distribution of intrinsic defects in a superconductor, and even different samples with an absolutely identical critical current can, with the introduction of artificial pinning centers, give both

an increase and a decrease in J_c, depending on the initial defects background. Therefore, the comparative studies of the effect of nanoinclusions on the critical characteristics of HTSC tapes should be performed only using identical superconducting matrices with the introduction of nanoinclusion in an identical way, which was done in this work.

There are different opinions in the literature about the effect of $BaSnO_3$ nanoinclusions on the density of critical current of HTSC films. Thus, it was shown in [12, 26] that an increase in the critical current of 2G HTSC tapes with $BaSnO_3$ can be observed only at low temperatures and high magnetic fields. At the same time, Oh et al [33] noticed a certain increase in the critical current at 77 K in GdBCO films, deposited on $SrTiO_3$ using PLD. This discrepancy with our results may be due, firstly, to different types of structures under study: the YBCO film grown on the multilayer tape and the GdBCO film on a $SrTiO_3$; secondly, to different methods of film synthesis: MOCVD and PLD; and, the last but not the least, to different methods of measuring the critical current: directly by transport and deducing from the DC magnetization loops, as done in [33]. Indeed, the introduction of nanoinclusions may increase the intragrain critical current (which affects the magnetization), and decrease the transport current due to a deterioration in the quality of the intergrain boundaries.

As for the EXAFS study [33], carried out to specify the pinning centers in GdBCO films, the results and conclusions cast some doubt. As we noted above, in the standard scheme of collecting spectra in the fluorescent mode, synchrotron radiation is directed normally to the surface of the film, which means that the polarization vector **E** is parallel to the film surface and hence, $\mathbf{E}\|ab$ if the HTSC film is grown on the substrate of $SrTiO_3(100)$. For this geometry, as shown in Section 3.2, the information extracted from the spectra relates to the average of Cu(2) – O(2,3) bonds in the *ab* plane and the Cu(1) – O(1) bond along the *b* axis, but not to the Cu(1) – O(4) bond along the *c* axis, which was selected by Oh et al. [33] in EXAFS spectra fitting.

It is worth noting that the $\mathbf{E} \parallel c$ orientation can be obtained if the film is grown on the $SrTiO_3(110)$ substrate, though the authors did not mention this. Let us assume that they indeed conducted research on such a film and obtained an EXAFS function from the contribution of Cu(1) – O(4) bonds along the *c* axis. In this case, the result obtained seems irrelevant, since, for example, a decrease in the coordination number of the Cu(1) – O(4) shell from N=2 to N≈1.3 in films with a thickness of 0.6 μm means the absence of an apical atom O(4) in every third unit cell of the lattice. Since O(4) is a structure-forming atom [48], such a film cannot exist.

It is generally known, that the oxygen deficiency in the YBCO (GdBCO) matrix is not associated with apical oxygen O(4), but with vacancies in the O(1) site in Cu(1)–O(1) chains along the *b* axis [48]. Therefore, the authors seem to make a mistake attributing the EXAFS data to the Cu(1)–O(4) bond, which does not contain any information about the local oxygen deficiency in the films, and has no relation to the film thickness. Thus, the conclusions of [33] concerning oxygen deficiency in O(4) as additional pinning centers seem to be incorrect.

Now let us estimate how a possible change in the occupancy of the O(1) site in

the matrix of $YBa_2Cu_3O_y$ (y=7-δ) affects the results of our EXAFS analysis given in Sec. 3.2.

Since the in-plane (**E**$\|ab$) polarized Cu K-edge EXAFS probes the Cu – O pair correlation averaged over Cu(2) – O(2,3) and Cu(1) – O(1) pairs, the contribution of Cu(1) – O(1) to the average coordination can be estimated as $(2y-4)/3$ [50]. Taking into account, that for our YBCO tapes with T_c=88.9 K, we can estimate the oxygen deficiency as $\delta \approx 0.19$ [48], and hence obtain $(2y-4)/3 \sim 15\%$. Since the contribution of the Cu(1)-O(1) bond to the EXAFS function of the averaged coordination Cu-O shell does not exceed 15%, even a significant change in the occupancy of the O(1) site (if possible) cannot have a noticeable effect on the Debye-Waller factor of the Cu – O bond, extracted from the EXAFS spectra and presented in Table 2 and Fig. 5.

5. Conclusion

The study of the dependence of the critical current of 2G HTSC tapes on the type of artificial pinning centers in the form of inert nanoinclusions showed that, despite the same perovskite structure and the same concentration (5 mol.%) of $BaSnO_3$ barium stannate and $BaZrO_3$ barium zirconate, their effect on critical parameters at 77 K is different. It is found that the $BaZrO_3$ nanoinclusions increase the critical current for both directions of the magnetic field relative to the tape surface, while the $BaSnO_3$ nanoinclusions reduce the critical current in both cases. Studies conducted by locally sensitive x-ray absorption spectroscopy methods EXAFS and XANES have shown that the nature of such a discrepancy is related to the different impact of BZO and BSO nanoinclusions on the local structure of the superconducting CuO_2 plane of the HTSC matrix. It is found that the $BaZrO_3$ nanoinclusions increase the stiffness of copper-oxygen bonds and minimize their static disorder in the YBCO matrix. On the contrary, the introduction of $BaSnO_3$ nanoinclusions leads to a significant increase in the static disorder of Cu – O bonds with a relatively weak effect on their stiffness. The results argue in favour of $BaZrO_3$ nanoinclusions (as opposed to $BaSnO_3$) as effective pinning centers for HTSC tapes used in superconducting devices operating at the boiling point of liquid nitrogen.

Acknowledgements

The authors acknowledge the ESRF Program committee (Grenoble, France) for providing the opportunity of XAFS measurements at the synchrotron facility. This work was supported by the Russian Federation represented by the Ministry of Science and Higher Education of the Russian Federation (Agreement No 075-15-2021-1352)

References

[1] Li Z Y, Li J, Wang Y, Yao Z, Kang Z R, Yuan B, Yang Z D, Jin Z and Hong Z 2016 *IEEE Trans. Appl. Supercond.* **26** 1–4

[2] Sung H-J, Park M, Go B-S and Yu I-K 2016 *Supercond. Sci. Technol.*, **29** 054001

[3] Vetrella U B, Celentano G, Marchetti M, Messina G, Morici L, Sabatino P, Viola R and della Corte A 2014 *IEEE Trans. Appl. Supercond.*, **24** 1–4

[4] Pan A V, Pysarenko S and Dou S X 2006 *Appl. Phys. Lett.*, **88** 232506

[5] Matsushita T, Isobe G, Kimura K, Kiuchi M, Okayasu S and Prusseit W 2008 *Supercond. Sci. Technol.*, **21** 054014

[6] Jones A, Al-Qurainy M, Hamood A, Lam S K H and Pan A V 2020 *Supercond. Sci. Technol.*, **33** 035004

[7] AL-Qurainy M M, Jones A, Rubanov S, Fedoseev S A, Rudnev I, Hamood A and Pan A V 2020 *Supercond. Sci. Technol.*, **33** 105006

[8] MacManus-Driscoll J L, Foltyn S R, Jia Q X, Wang H, Serquis A, Civale L, Maiorov B, Hawley M E, Maley M P and Peterson D E 2004 *Nat. Mater.*, **3** 439–443, may 2004.

[9] Mele P, Matsumoto K, Horide T, Ichinose A, Mukaida M, Yoshida Y, Horii S and Kita R 2008 *Supercond. Sci. Technol.*, **21** 032002

[10] Bartůněk V and Smrčková O 2010 *Ceram. Silik.*, **54** 01

[11] Boytsova O V, Samoilenkov S, Vasiliev A, Kaul A, Kalinov A and Voloshin I 2019 *ECS Trans.*, **25** 1185–1190

[12] Samoilenkov S V, Boytsova O V, Amelichev V A and Kaul A R 2011 *Supercond. Sci. Technol.*, **24** 055003

[13] Zhou H, Maiorov B, Baily S A, Dowden P C, Kennison J A, Stan L, Holesinger T G, Jia Q X, Foltyn S R and Civale L 2009 *Supercond. Sci. Technol.*, **22** 085013

[14] Wimbush S C, Walsh D and Hall S R 2010 *Physica C*, **470** 373–377

[15] H. Kobayashi, S. Ishida, K. Takahashi, M. Konishi, A. Ibi, S. Miyata, Y. Yamada, Y. Shiohara, T. Kato and T. Hirayama Investigation of magnetic properties of YBCO film with artificial pinning centers on PLD/IBAD metal substrate. *Physica C*, 445-448:625–627, oct 2006.

[16] Kaneko K et al 2010 *J. Appl. Phys.*, **108** 063901

[17] Teranishi R, Konya K, Inoue M, Sato Y, Kaneko K, Izumi T and Satoshi Awaji S 2018 *IEEE Trans. Appl. Supercond.*, **28** 1–5

[18] Choi S M, Shin G M and Yoo S I *Physica C*, **485** 154–159

[19] Maroni V A, Kropf A J, Aytug T and Paranthaman M 2009 *Supercond. Sci. Technol.*, **23** 014020

[20] Selvamanickam V et al 2009 *Supercond. Sci. Technol.*, 23(1):014014

[21] Hapipi N M, Chen S K, Shaari A H, Kechik M M A, Tan K B, Lim K P and Lee O J 2018 *J. Supercond. Novel Magn.*, **32** 1191–1198

[22] Prayoonphokkharat P, Amonpattaratkit P and Watcharapasorn A 2020 *Appl. Phys. A-Mater.*, **126** 140

[23] Maiorov B, Baily S A, Zhou H, Ugurlu O, Kennison J A, Dowden P C, Holesinger T G, Foltyn S R and Civale L 2009 *Nat. Mater.*, **8** 398–404

[24] Sebastian M A, Ebbing C, Zhang W, Huang J, Wang H, Chen S, Gautum B, Wu J and Haugan T 2017 *IOP Conf. Ser.: Mater. Sci. Eng.*, **279** 012031

[25] Pižl M, Jankovský O, Ulbrich P, Szabó N, Hoskovcová I, Sedmidubský D and Bartůněk V. 2017 *J. Organomet. Chem.*, **830** 146–149

[26] Chepikov V et al 2017 *Supercond. Sci. Technol.*, **30** 124001

[27] Chepikov V et al 2017 *IEEE Trans. Appl. Supercond.*, **27** 1–5

[28] Rizzo F 2020 *Supercond. Sci. Technol.*, **33** 030501

[29] Kochat M, Pratap R, Galstyan E, Majkic G and Selvamanickam V 2019 *IEEE Trans. Appl. Supercond.*, **29** 1–4

[30] Majkic G, eong J S, Yun H, Hernandez F C R, Galstyan E, Pratap R, Cheng H, Stokes A, Mkhoyan K A and Selvamanickam V 2021 *Supercond. Sci. Technol.*, **34** 115002

[31] Khan M Z, Malmivirta M, Zhao Y, Wu X, Jha R, Awana V P S, Huhtinen H and Paturi P 2018 *Physica C*, **555** 15–23

[32] Lei L, Li L, Wang X, Zhang Z, Zhao G, Jia J, Yan F, Duan Z, Jin L, Li C and Zhang P 2020

Prog. Nat. Sci.: Mater. Int., **30** 180–184
[33] Oh J Y, Kang W N and Kang B 2019 *J. Supercond. Novel Magn.*, **32** 3165–3170
[34] A P Menushenkov A P et al 2017 *Supercond. Sci. Technol.*, **30** 045003
[35] O. Mathon O et al 2015 *J. Synchrotron Radiat.*, **22** 1548–1554
[36] d'Acapito F, Trapananti A and Puri A 2016 *J. Phys. Conf. Ser.*, **712** 012021
[37] Booth C and Bridges F 2003 *Phys. Scr.*, **T115**, 07
[38] Klementev K V 2001 *J. Phys. D: Appl. Phys.*, **34** 209–217
[39] Newville M 2001 *J. Synchrotron Radiat.*, **8** 322–324
[40] Dew-Hughes D 1974 *Philos. Mag.*, **30** 293–305
[41] Lanzara A, Zhao G M, Saini N L, Bianconi A, Conder K, Keller H and Müller K A 1999 *J. Phys.: Condens. Matter*, **11** L541–L546
[42] Bianconi A 2020 Many-body quantum physics in XANES of highly correlated materials, mixed-valence oxides and high-temperature superconductors *X-ray absorption spectroscopy and related techniques* (*International Tables for Crystallography* vol *I*) ed C T Chantler et al (International Union of Crystallography)
[43] Temprano D, Mesot J, Janssen S, Conder K, Furrer A, Mutka H and Müller K 2000 *Phys. Rev. Lett.*, **84** 1990–3
[44] Menushenkov A, Kuznetsov A, Chernikov R, Ivanov A, Sidorov V and Klementiev K 2010 *Z. Krist. - Cryst. Mater.*, **225** 487–491
[45] Menushenkov A P, Kuznetsov A V, Chernikov R V, Ivanov A A, Sidorov V V and Klementiev K V 2013 *J. Supercond. Novel Magn.*, **27** 925–928
[46] Sevillano E, Meuth H and Rehr J J 1979 *Phys. Rev. B*, **20** 4908–4911
[47] Rehr J J, Kas J J, Vila F D, Prange M P and Jorissen K 2010 *Phys. Chem. Chem. Phys.*, **12** 5503–5513
[48] Jorgensen J D, Veal B W, Paulikas A P, Nowicki L J, Crabtree G W, Claus H and Kwok W K 1990 *Phys. Rev. B*, **41** 1863–1877
[49] Menushenkov A P, Popov V V, Gaynanov B R, Ivanov A A, Kuznetsov A V, Yaroslavtsev A A, d'Acapito F and Puri A 2019 *JETP Lett.*, **109** 529–535
[50] Oyanagi H, Saini N L and Bianconi A 2000 *Int. J. Mod. Phys. B*, **14** 3623–3631